

Retraction

Retracted: Fast Extraction Algorithm for Local Edge Features of Super-Resolution Image

Security and Communication Networks

Received 5 December 2023; Accepted 5 December 2023; Published 6 December 2023

Copyright © 2023 Security and Communication Networks. This is an open access article distributed under the Creative Commons Attribution License, which permits unrestricted use, distribution, and reproduction in any medium, provided the original work is properly cited.

This article has been retracted by Hindawi, as publisher, following an investigation undertaken by the publisher [1]. This investigation has uncovered evidence of systematic manipulation of the publication and peer-review process. We cannot, therefore, vouch for the reliability or integrity of this article.

Please note that this notice is intended solely to alert readers that the peer-review process of this article has been compromised.

Wiley and Hindawi regret that the usual quality checks did not identify these issues before publication and have since put additional measures in place to safeguard research integrity.

We wish to credit our Research Integrity and Research Publishing teams and anonymous and named external researchers and research integrity experts for contributing to this investigation.

The corresponding author, as the representative of all authors, has been given the opportunity to register their agreement or disagreement to this retraction. We have kept a record of any response received.

References

- [1] F. Chen and B. Yang, "Fast Extraction Algorithm for Local Edge Features of Super-Resolution Image," *Security and Communication Networks*, vol. 2022, Article ID 8801978, 10 pages, 2022.

Research Article

Fast Extraction Algorithm for Local Edge Features of Super-Resolution Image

Feng Chen  and Botao Yang 

Rongcheng Campus, Harbin University of Science and Technology, Harbin 150080, China

Correspondence should be addressed to Feng Chen; chenfeng@hrbust.edu.cn

Received 21 October 2021; Revised 7 December 2021; Accepted 10 December 2021; Published 5 January 2022

Academic Editor: Chinmay Chakraborty

Copyright © 2022 Feng Chen and Botao Yang. This is an open access article distributed under the Creative Commons Attribution License, which permits unrestricted use, distribution, and reproduction in any medium, provided the original work is properly cited.

Image super-resolution is getting popularity these days in diverse fields, such as medical applications and industrial applications. The accuracy is imperative on image super-resolution. The traditional approaches for local edge feature point extraction algorithms are merely based on edge points for super-resolution images. The traditional algorithms are used to calculate the geometric center of gravity of the edge line when it is near, resulting in a low feature recall rate and unreliable results. In order to overcome these problems of lower accuracy in the existing system, an attempt is made in this research work to propose a new fast extraction algorithm for local edge features of super-resolution images. This paper primarily focuses on the super-resolution image reconstruction model, which is utilized to extract the super-resolution image. The edge contour of the super-resolution image feature is extracted based on the Chamfer distance function. Then, the geometric center of gravity of the closed edge line and the nonclosed edge line are calculated. The algorithm emphasizes on polarizing the edge points with the center of gravity to determine the local extreme points of the upper edge of the amplitude-diameter curve and to determine the feature points of the edges of the super-resolution image. The experimental results show that the proposed algorithm consumes 0.02 seconds to extract the local edge features of super-resolution images with an accuracy of up to 96.3%. The experimental results show that our proposed algorithm is an efficient method for the extraction of local edge features from the super-resolution images.

1. Introduction

The super-resolution technology of images is a technique for obtaining high-resolution images corresponding to scenes by using an existing method for low-resolution images without changing the image observation system [1]. Image super-resolution technology is improving day by day due to the huge demand in computer science and aligned fields [2]. It is widely used in medical imaging, video surveillance and transmission, generation of satellite remote sensing images, and HDTV [3]. In order to process images and to draw meaningful inferences, it is necessary to extract the edge's local features of super-resolution images [4]. In this paper, the features of super-resolution images are extracted fast from the point of view of local feature points. Since the points are the primitives that constitute the super-resolution

image, the points constituting the image vary widely. Therefore, it needs to extract some specific features that can represent the image attributes and can assist in image feature extraction and recognition. Feature extraction is also important to identify and track the target according to different needs and to construct a three-dimensional target surface [5, 6]. In the past research endeavours, many feature point extraction algorithms are proposed and deployed, which are mainly divided into two categories. One is the curvature-based local edge feature extraction algorithm of super-resolution image, and the other is the grey gradient-based algorithm. Both algorithms have disadvantages. The first type of algorithm has a large amount of calculation, and the second type of algorithm has low accuracy. At present, there is a feature point extraction algorithm based on edge points. Compared with the performance of the first two types of

algorithms, the algorithm is simple and convenient to implement, but it has the following problems: first, only the edge line is considered. It is closed and does not conform to the actual situation. Secondly, the obtained local edge features of the super-resolution image are only the convex curvature with large curvature on the edge line, and the description of the shape of the target is incomplete [7].

In [8], the authors have introduced a novel method for extracting transform characteristics from pictures or video frames. These characteristics are used to represent the local visual content of image and video frames. The projected method, such as Shot Boundary Detection (SBD), is measured using conventional methods utilizing the standard procedure. The experimental results reveal that the proposed method outperforms previous methods in terms of computational cost. In [9], the authors have investigated various picture feature extraction analysis techniques. By aggregating low-level characteristics to explore various feature data representations, this technique obtains more expressive and productive high-level information content. In [10], the authors have suggested a random deep neural network-based picture feature extraction technique. The goal of this strategy is to detect more consistent features by eliminating duplicate feature points. In [11], the authors have introduced a novel approach based on Bidimensional Empirical Mode Decomposition. This method was used to extract self-adaptive characteristics from pictures. In [12], the authors have designed a video summarization framework based on frame choice to determine only significant frames. As there are various drawbacks in the existing systems, we aim to produce an efficient algorithm to solve the above problems, which is fast and efficient than the previous approaches for local edge feature extraction of super-resolution images. The proposed algorithm will accurately reflect the shape contour of the target feature, which has important significance to extract the super-resolution image features.

The contribution of the work is as follows:

- (i) In this paper, a new fast extraction algorithm for local edge features of super-resolution images is proposed
- (ii) The algorithm mainly focuses on the super-resolution image reconstruction model, which is used to obtain the super-resolution image
- (iii) The algorithm puts emphasis on polarizing the edge points with the center of gravity as the pole to find the local extreme points of the upper edge of the amplitude-diameter curve and determine the feature points of the edge of the super-resolution image
- (iv) The algorithm is compared using a super-resolution image reconstruction model and local edge feature extraction of a super-resolution image on the basis of which we calculate the geometric center of gravity and polarization of edges
- (v) So, the proposed algorithm produces efficient output than the existing traditional approaches

when compared using the RPC curve and keeping F -measure as a calculatory parameter

- (vi) The proposed algorithm gives an efficiency of around 99% that surpasses the traditional approaches with a great margin, which was about 75% and 64%, respectively

Further, the paper is divided into five sections:

- (1) Section 1 gives an introduction about the existing approaches and shows the drawbacks of existing approaches
- (2) Section 2 shows the various approaches to the image reconstruction model and local edge feature extraction model and the changes to be made in them to make them efficient
- (3) Section 3 shows us the comparative result analysis of various algorithms with respect to the proposed system
- (4) Section 4 is the discussion of results and the various approaches made to make the algorithm efficient
- (5) Section 5 tells us about the obtained results and how much efficient our approach is with respect to others

2. Material and Methods

2.1. Super-Resolution Image Reconstruction Model. Degraded models for super-resolution image reconstruction can be expressed as follows:

$$y_k = DW_k F_k X + \eta_k, \quad (1)$$

where y_k is the degraded k th frame image, X is the high-resolution image, D and W_k are the downsampling matrix and motion matrix, F_k is the fuzzy matrix, and η_k is the noise.

Let the low-resolution image be Y and the corresponding high-resolution image be X . The problem that the super-resolution reconstruction needs to solve is to find the optimal approximate solution X under the condition of known Y . The common method for solving this problem is Maximum Posterior Probability (MAP) under low-resolution range image conditions. MAP estimates can be represented by

$$\hat{x} = \arg \max_X P(X|Y_1, \dots, Y_N). \quad (2)$$

According to the Bayesian estimation criterion, (2) can be rewritten as follows:

$$\hat{x} = \arg \max_X P(Y_1 = y_1, \dots, Y_N = y_N | X = x) P(X = x). \quad (3)$$

In (3), it is assumed that the noise is independent Gaussian white noise [10] and the variance is σ^2 . Then, (4) is expressed as follows:

$$P(Y_1 = y_1, \dots, Y_N = y_N | X = x) = \frac{1}{(2\pi\sigma^2)^{N_1 N_2}} \times \exp\left(-\sum_{k=1}^N \frac{\|y_k - DW_k F_k X\|_2^2}{2\sigma^2}\right). \quad (4)$$

According to the Markov random field model, the prior probability $P(X = x)$ of the high-resolution range image is obtained, and the equivalence between MRF and Gibbs is used. The Gibbs distribution is used to explicitly describe the Markov distribution; that is, the prior probability of X can be expressed by

$$P(X = x) = \frac{1}{Z} \exp\left(-\frac{1}{T} \sum_{c \in C_X} V_c^x(x)\right). \quad (5)$$

The energy function takes the form of Li, as follows:

$$\begin{aligned} \sum_{c \in C_X} V_c^x(x) = & \sum_{i=1}^{L_1} \sum_{j=1}^{L_2} 4\gamma - \\ & \gamma \exp\left\{\frac{-[x(i, j) - x(i, j-1)]^2}{\gamma}\right\} - \\ & \gamma \exp\left\{\frac{-[x(i, j) - x(i, j+1)]^2}{\gamma}\right\} - \\ & \gamma \exp\left\{\frac{-[x(i, j) - x(i-1, j)]^2}{\gamma}\right\} - \\ & \gamma \exp\left\{\frac{-[x(i, j) - x(i+1, j)]^2}{\gamma}\right\}. \end{aligned} \quad (6)$$

Here, Z is a normalized constant, T is the temperature parameter, and $V_c^x(x)$ is the potential function of the connected group; the potential function describes the interaction of a set of neighbouring pixels, and different potential functions determine the different MRF models. From (4) and (5), (3) can be rewritten as follows:

$$\hat{x} = \arg \min_X \left(\sum_{k=1}^N \|y_k - DW_k F_k X\|_2^2 + \sum_{c \in C_X} V_c^x(x) \right). \quad (7)$$

Since the energy function of the prior distribution of the DAMRF model is a nonconvex function when solving the optimal solution of the objective function, it is easy to fall into the local minimization problem, and the optimal approximate solution of the reconstructed image cannot be obtained [7, 11]. Therefore, the graduated nonconvexity (GNC) optimization algorithm is used to optimize the objective function to obtain the optimal solution of the reconstruction result.

2.2. Local Edge Feature Extraction of Super-Resolution Image

2.2.1. Chamfer Matching Metrics. The Chamfer distance is used to measure the similarity of the two-edge figures. The match between the template map T and the image to be

matched E is achieved by searching for their minimum Chamfer distance. The main steps are as follows:

Step 1. Calculate the Chamfer distance map of the image to be matched.

Step 2. Superimpose the template on the distance map. Calculate the Chamfer distance between the template and the image to be matched as follows:

$$D_{\text{Chamfer}} = \left(\frac{1}{n}\right) \sum_{i=1}^n v_i. \quad (8)$$

Here, n is the number of edges of the template and v_i is the distance value at which the template is superimposed.

Step 3. The template is translated on the distance map to obtain the Chamfer distance value distribution function $S(p)$ of the template on the image to be matched, and the position vector p of the minimum value $S(p)$ is the best matching point. In practical applications, image features are extracted by determining whether the minimum value $S(p)$ is less than a set threshold θ .

2.2.2. Local Edge Contour Feature Function Based on Class Chamfer Distance. The local edge features used in this paper are defined by a rectangular window, that is, $r = (x, y, w, h)$. Each local edge r is represented by two positional parameters (x, y) and two scaled parameters (w, h) , which, respectively, represent the width and height of the rectangle. The local edge feature F_r is defined on the Chamfer distance map I of the image, concerning (8), and the eigenvalue calculation is as follows:

$$F_r(I) = \frac{1}{w \times h} \sum_{i=x}^{x+w} \sum_{j=y}^{y+h} v_{i,j}, \quad (9)$$

where $v_{i,j}$ is the value of the Chamfer distance at the corresponding point in the image.

This paper implements the fast calculation of (9) by establishing the integrated image of the Chamfer distance map. For the distance graph I , as shown in Figure 1, the integral image value at a pixel (x, y) is defined as $ii(x, y) = \sum_{x_1 \leq x, y_1 \leq y} i(x_1, y_1)$, that is, the sum of all the pixel values of the shaded portion. Once the integral image is established, the local edge feature values of any parameters can be obtained by only 4 table lookups and simple operations.

The super-resolution feature extracted by the above method is the feature edge contour, so the geometric center of gravity of the feature contour needs to be calculated to determine the feature points that meet the requirements.

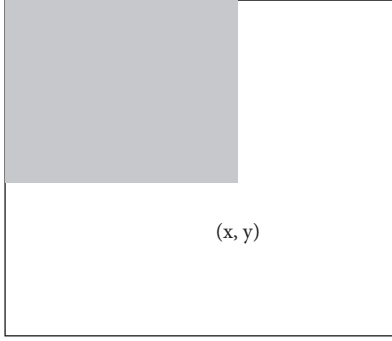


FIGURE 1: Integral image value at the point (x, y) .

2.3. Geometric Center of Gravity Calculation. The geometric center of gravity is obtained by weighting the points in the Grassmannian space and adding them; then it is divided by the sum of ownership. There are many state-of-the-art approaches that deal with calculation of geometric center of gravity [13, 14]. The pixel points of the image have greyscale properties, but the feature points extracted in this paper are on the edge contour line, and the edge image is a binary plane image, which is independent of the grey level of the image. Therefore, the edge image can be considered as a uniform substance. So, the geometric center of gravity of the edge contour is the geometric center.

Considering whether the extracted edge lines are closed, the edge contours can be divided into two categories: closed contours and nonclosed contours, and their centres of gravity are calculated below.

(1) *Calculation for the Geometric Center of Gravity of the Closed Contour.*

For a closed irregular planar figure, let the coordinates of the edge points be (x_i, y_i) and $1 \leq i \leq n$ be the number of edge points. The geometric center coordinate (x_0, y_0) is calculated by

$$x_0 = \frac{1}{n} \sum_{i=1}^n x_i, y_0 = \frac{1}{n} \sum_{i=1}^n y_i. \quad (10)$$

The geometric center of gravity, thus, obtained is unique. The experimental results are shown in Figure 2(a). In the figure, the circle represents the center of gravity of the geometry, and the contour of the feature extraction is closed.

(2) *Calculation for the Geometric Center of Gravity of the Unclosed Contour.*

Since the three points that are not collinear on the plane are linearly independent, the coordinates for the center of gravity of the triangle are uniquely defined [15, 16]. Therefore, for a convex or concave curve, it can first form a triangle consisting of the two ends of the edge line and the middle point and then find the geometric center of gravity. If an edge line is not single convex or single concave, then it is segmented. The experimental results are shown in Figure 2(b). In the figure, the curve AC is divided into segments from point B , and the geometric centers of gravity of the arcs AC and BC are, respectively, obtained. The solid

line is the outline of the feature extraction, which is non-closed, and the circle represents the center of gravity of the geometry.

2.4. Polarization of Edge Points. To conveniently calculate the length and position of each point on the edge from the geometric center of gravity, it is necessary to polarize the edge point. Taking the geometric center of gravity as the pole, as shown in Figure 3, the conversion equation is as follows:

$$\begin{cases} \rho_i = \sqrt{(x_i - x_0)^2 + (y_i - y_0)^2} \\ \theta_i = \arctan\left(\frac{y_i - y_0}{x_i - x_0}\right) \end{cases} \quad (11)$$

In Figure 3, the origin of the coordinates is represented by (x_0, y_0) , and the points in polar coordinates are represented by (x_i, y_i) .

The polarized edge points form a polar-amplitude curve, as shown in Figure 4. In Figure 4, the abscissa is the edge point angle, and the unit is the arc degree; the ordinate is the polar diameter of the edge point, and the unit is taken in micrometres (μm). The horizontal and vertical coordinates' contents in Figures 5 to 8 are the same as those in Figure 4.

2.5. Determination of the Local Feature Points of the Image Edge. Polarization simplifies the problem, making it easy to find extreme points locally and then further identifying the feature points [17, 18]. The extraction process of extreme points and feature points is described below.

2.5.1. Determination of the Extreme Point. If the maximum point in the range $[\theta_1, \theta_2)$ is represented by P_{\max} , then P_{\max} can be described by

$$P_{\max} = \max_{\theta \in [\theta_1, \theta_2]} (\rho). \quad (12)$$

Similarly, if the minimum value point in the range $[\theta_1, \theta_2)$ is represented by P_{\min} , then P_{\min} can be represented by

$$P_{\min} = \min_{\theta \in [\theta_1, \theta_2]} (\rho). \quad (13)$$

The curves of the local maximum point and the minimum point on the polar-amplitude curve are shown in Figures 5 and 6, respectively, and the interval between the two figures is 10° , that is, $1/18(\pi)$. In Figure 5, the maximum value of the local maximum point is about $140 \mu\text{m}$, and the minimum value is about $20 \mu\text{m}$. In Figure 6, the maximum value of the local maximum point is about $110 \mu\text{m}$, and the minimum value is about $15 \mu\text{m}$.

2.5.2. Determination of Feature Points. The final feature points are obtained based on the principle of nonmaximum (small) value suppression in the local area [19, 20].

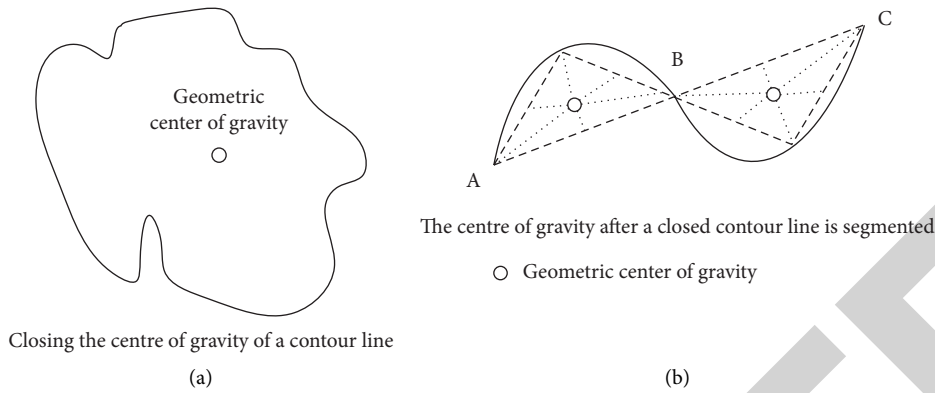


FIGURE 2: The geometric barycenter of the contour line of an object. (a) Closing the center of gravity of a contour line. (b) The center of gravity after a closed contour line is segmented.

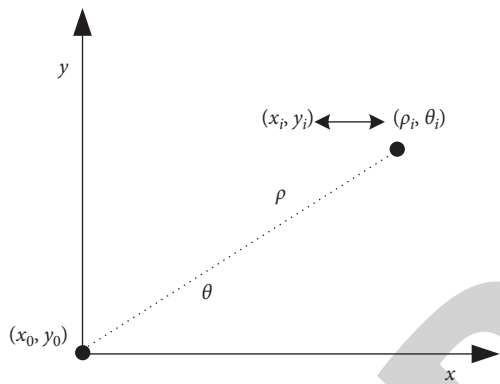


FIGURE 3: Polar coordinates of edge points.

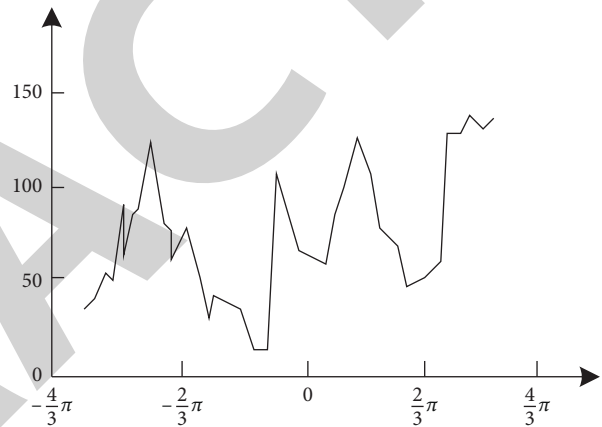


FIGURE 5: Polar diameter and amplitude curves of local maximum points.

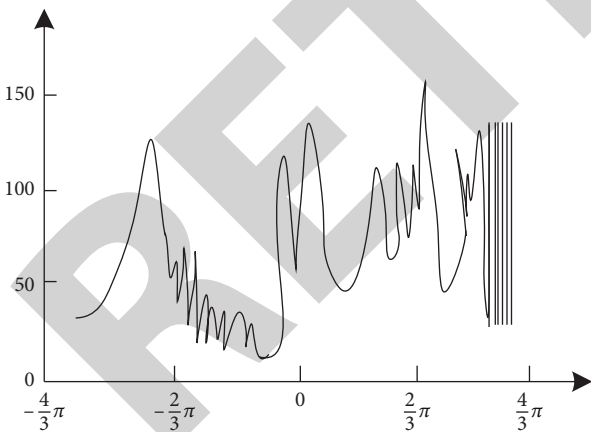


FIGURE 4: Polar diameter curve.

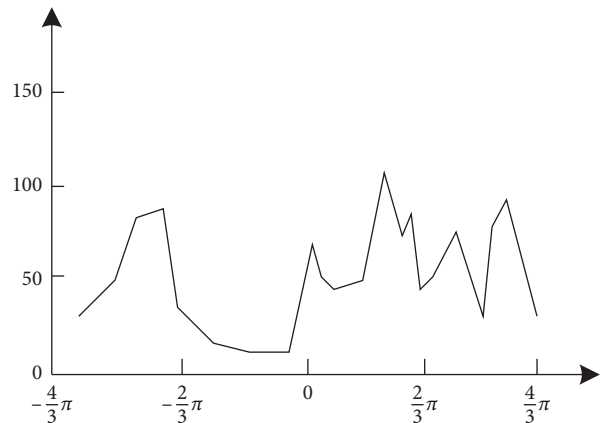


FIGURE 6: The polar diameter curve of the local minimum point.

Therefore, the maximum (small) value point of each interval and the maximum (small) value point in the adjacent interval are compared, and if the polar diameter of the maximum (minimum) value point is larger (smaller) than that of the maximum (minimum) value point in the two adjacent intervals, it is considered to be a feature point. The argument-polar radius curves of the two feature points further extracted from the maximum and minimum values

of Figures 5 and 6 are shown in Figure 7, and the finally extracted feature points are as shown in Figure 8 in Figure 7; the argument-polar radius curve of the maximum value curve is always above the argument-polar radius curve of the minimum value curve; the distribution of the last extracted effective feature points and the argument-polar radius curve

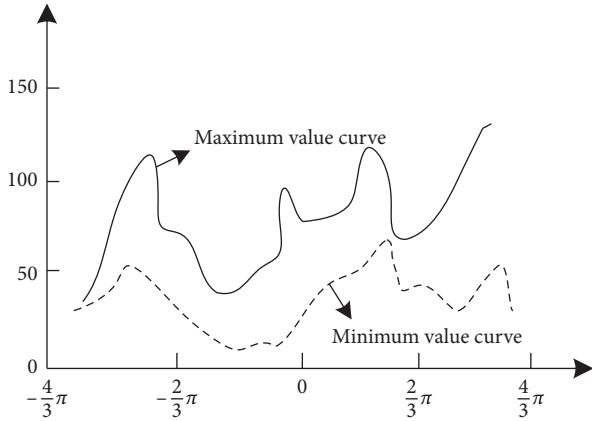


FIGURE 7: The maximum diameter curve of the maximum diameter (small) value.

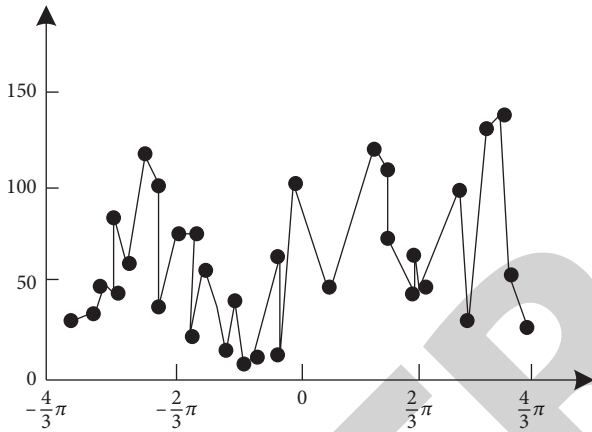


FIGURE 8: The polar diameter curve diagram of the edge local feature points.

of the feature points can be seen in Figure 7. In Figure 8, it can be observed obviously that the polar diameter curve diagram of the edge local feature points varies from the range of $-4/3\pi$ to $4/3\pi$, representing the values of maximum value curve points and the minimum value curve points on the y -axis ranging from 0 to 150.

3. Results

3.1. Algorithm Validation. To verify the effectiveness of the proposed algorithm, the expansion feature extraction test of a single super-resolution image is selected. Figure 9 is the local edge feature result of the super-resolution image extracted by the proposed algorithm. It can be seen from the analysis of Figure 9 that the algorithm not only extracts the feature points of the super-resolution image convex, but also the feature points of the concave point can be detected. The connection of these feature points can reflect the edge contour shape of the target, which verifies the validity of the local edge features extraction by the proposed algorithm.

To verify the effectiveness of the proposed algorithm, the advantages of the proposed algorithm are highlighted. The

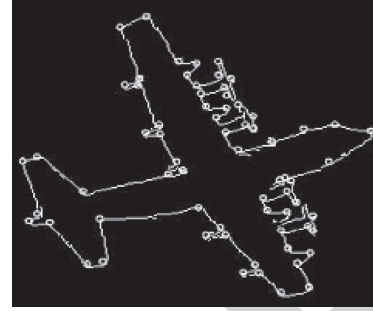


FIGURE 9: The feature points extracted by this algorithm.

super-resolution image of the valve pressure gauge is used as the object and 10% noise is added. The proposed algorithm, method given in paper [4], and method given in paper [5] are used to extract local edge features of the image. The original super-resolution image of the pressure meter with 10% noise is shown in Figure 10(a), and the result of feature extraction is shown in Figures 10(b)–10(d).

Figure 10(b) is the result of the method given in paper [4] extracting the local edge features of the super-resolution image, and Figure 10(c) is the extraction result of the method given in paper [5]. Due to the feature points extracted by the two algorithms being unclear, they are circled with red lines.

3.2. Comparison of RPC Performance and F-Measure Performance of Different Algorithms

3.2.1. Testing Set. To highlight the advantages of the proposed algorithm, it is compared with the method given in paper [4] and the method given in paper [5]. The experiment uses the super-resolution image database of vehicles in UIUC. The database consists of a training set and a testing set. The training set includes 550 positive samples with size of 100×40 . The experiment does not increase the number of positive samples in the training set (usually, increasing the number of training samples can improve the accuracy of the classifier), and the testing set consists of two subsets, denoted by T_I and T_{II} , respectively. T_I contains 170 super-resolution images with a total of 200 vehicles. The scale of vehicle imaging is the same as the training set. T_{II} contains 108 super-resolution images with 139 vehicles. The scale of vehicle imaging is different from the T_I testing set. The range is between 0.8 and 2 times. Some testing images contain complex backgrounds. Some images also have partial occlusion and image blur. In general, the feature extraction of testing set T_{II} is more difficult than that of testing set T_I . The training set also includes 50,517 negative samples, each of which is 100×40 in size.

The experiment uses the recall rate, precision rate, and F -measure to evaluate the performance of the algorithm. The calculation method of the evaluation index is as follows:

- (1) The recall-precision curve (RPC) is defined as follows:

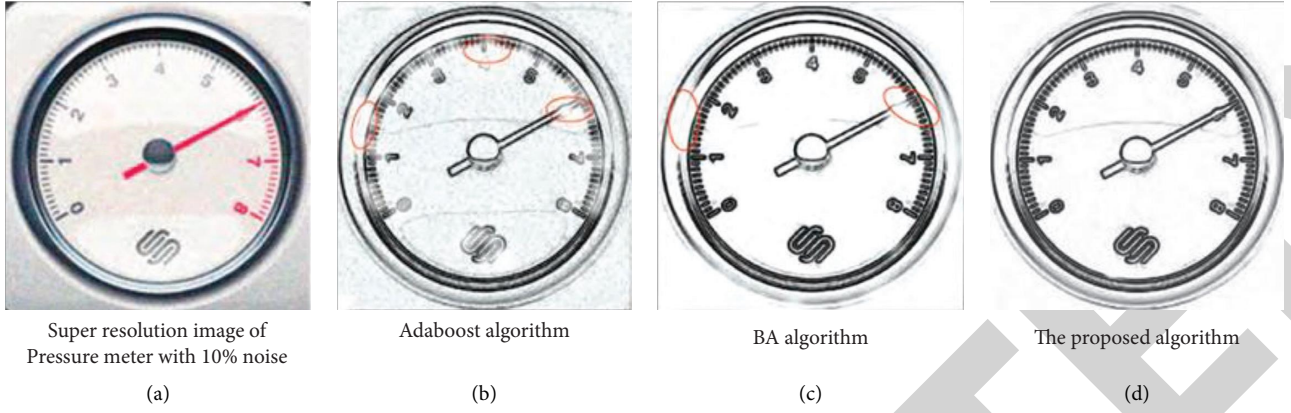


FIGURE 10: Local edge feature extraction results from noisy super-resolution images.

$$\text{recall} = \frac{P_T}{P_n}, \quad (14)$$

$$\text{precision} = \frac{P_T}{P_T + P_F}. \quad (15)$$

In the equation, P_T , P_F , and P_n , respectively, indicate the number of correct extraction of features, the number of error extractions, and the total number of features.

- (2) The F -measure (F _measure) is defined as (16), which can be considered as an equal error measure:

$$F_measure = \frac{2\text{recall} \times \text{precision}}{\text{recall} + \text{precision}}. \quad (16)$$

3.2.2. Analysis of Experimental Results. During the experiment, some feature extraction results of the proposed algorithm are shown in Figures 11(a)–11(c).

It can be seen from Figures 11(a)–11(c) that the result of using the algorithm of this paper to extract the vehicle in the super-resolution image can identify the vehicle in the image in the case of obstacle occlusion and verify the effectiveness of the algorithm.

The feature extraction and RPC fold line comparison of the three algorithms in the testing set T_I are shown in Table 1 and Figure 12, respectively. The feature extraction and RPC fold line comparison of the three algorithms in the testing set T_{II} are shown in Table 2 and Figure 13, respectively.

In Table 1, the equal error measure of the proposed algorithm is 96.3%, which is 14.1% higher than that of the method given in paper [4] and 21.1% higher than that of the method given in paper [5]. The average feature extraction time of the proposed algorithm is 0.02 s, which saves 0.075 s compared with the method given in paper [4] and 0.036 s compared with the method given in paper [5].

In Figure 12, the RPC polyline arrangement of the proposed algorithm, method given in paper [4], and the method given in paper [5] can be seen. The RPC polyline of the proposed algorithm is located at the top of the line graph. The initial value of the algorithm is 60%. The rate rises

linearly, the stability is about 97% in the later period, and the maximum precision is 99%; the initial value of the method given in paper [4] and the method given in paper [5] is about 8%. The maximum precision of the method given in paper [4] is about 75% and that of the method given in paper [5] is approximately 64%. From this, we can clearly state that our proposed algorithm is better in terms of precision compared to the method given in paper [4] and the method given in paper [5] as our algorithm has the maximum of 99% precision rate at its best case and the other algorithms method given in paper [4] and method given in paper [5] are having a maximum of 75% and 64% approximately as our proposed algorithm outcasts them in case of RPC curves.

It can be seen from Table 2 that the F -measure value of the proposed algorithm is higher, and the average feature extraction time is less. Compared with the case of Table 1, the proposed algorithm saves feature extraction time and has high efficiency while maintaining the highest accuracy and high precision.

In Figure 13, the RPC polyline of the proposed algorithm on the testing set T_{II} is located at the top of the image, indicating that the RPC performance of the proposed algorithm is the strongest. Like the testing set T_I , the initial value of the proposed algorithm is 60%, which is larger than that of the method given in paper [4] of 51% and the method given in paper [5], respectively; the highest precision of the proposed algorithm is 99%, and the highest precision of the method in paper [4] and the method in paper [5] is 82% and 68%, respectively. Comparing the three groups of data, the RPC performance of the proposed algorithm is superior to similar algorithms and has significant advantages.

4. Discussion

In Figure 10, the feature points extracted by the method given in paper [4] and the method given in paper [5] have a commonality: fuzzy, unclear, and large fragment points; it is difficult to effectively restore the local edge features of super-resolution images, affecting the image analysis effect; relatively speaking, the feature points extracted by the proposed algorithm in Figure 10(d) are clear and significant. The pointers and meter scales of the pressure gauge are clear and

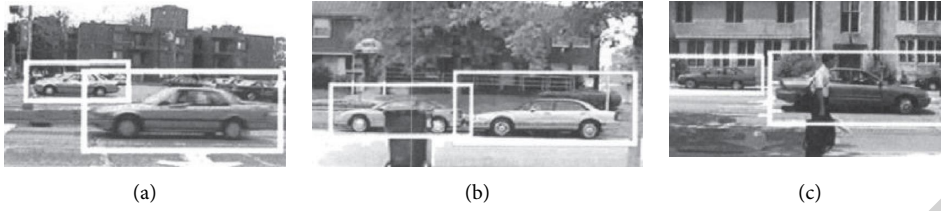
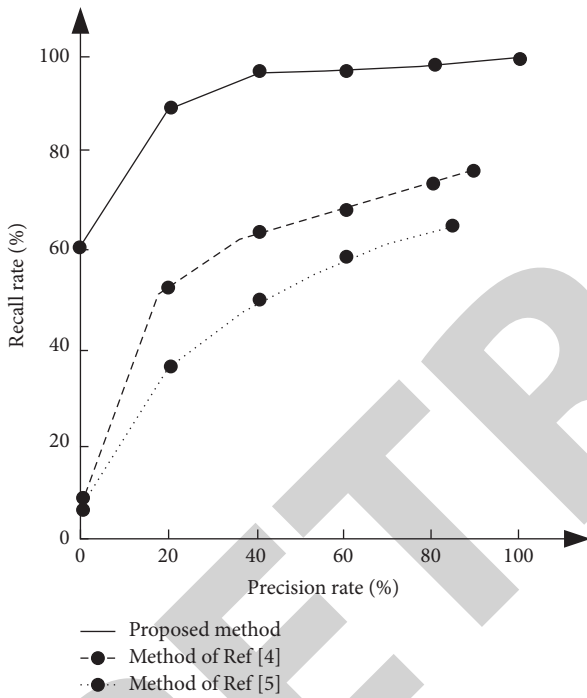


FIGURE 11: Part of the feature extraction results of the algorithm.

TABLE 1: Feature extraction of different algorithms on the test set T_I .

Algorithm	Number of base classifiers	F -measure (%)	Average feature extraction time (s)	Test platform
Method of paper [4]	800	82.2	0.095	1.86 GHz Core 2 Duo
Method of paper [5]	4050	75.2	0.056	1.86 GHz Core 2 Duo
Proposed method	1850	96.3	0.02	1.86 GHz Core 2 Duo

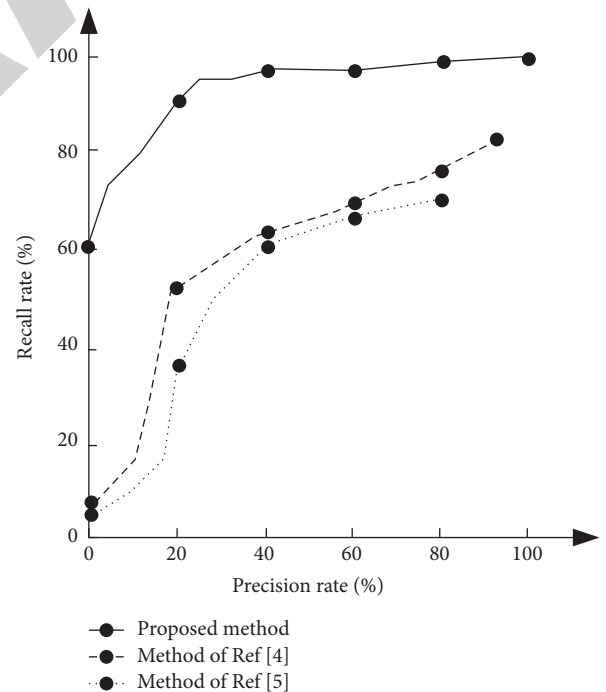
FIGURE 12: Comparison of RPC curves of three algorithms on T_I .

complete, and there are only weak blur points at the edge of the instrument, which does not affect the overall image restoration effect. In summary, the proposed algorithm can effectively extract the feature points of a super-resolution image with 10% noise, and the acquired local edges features are clear, continuous, and complete.

Based on the obtained local features of the super-resolution image, the proposed algorithm calculates the geometric center of gravity of the closed contour line and the nonclosed contour line to further determine the effective feature points. Firstly, the edge points are polarized, which is convenient for calculating the length and position of each point on the edge point from the geometric center of gravity, searching for local extremum points, and further determining the feature points so that the feature points of the

TABLE 2: Feature extraction performance of different algorithms on the test set T_{II} .

Algorithm	F -measure (%)	Average feature extraction time (s)
Method in paper [4]	44	0.35
Method in paper [5]	80.1	0.22
Proposed method	95.6	0.031

FIGURE 13: Comparison of RPC algorithms for three algorithms on the test set T_{II} .

obtained super-resolution image are effective and reliable. The final feature points are obtained on the principle of nonmaximum (minimum) value suppression in the local area.

In Table 1, the equal error measure of the proposed algorithm is 96.3%, which is 14.1% higher than that of the method given in paper [4] and 21.1% higher than that of the method given in paper [5]. The equal error measure indicates the accuracy of feature extraction, which indicates the accuracy of the proposed algorithm to extract the local edge features of the super-resolution image is high; the average feature extraction time of the proposed algorithm is 0.02 s, which saves 0.075 s compared with the method given in paper [4] and 0.036 s compared with the method given in paper [5]. It can be seen that the average time of extracting features by using the proposed algorithm is less. In summary, compared with similar algorithms, the proposed algorithm extracts feature with the shortest time while maintaining the highest accuracy and achieves fast feature extraction with high efficiency and high precision.

In Figure 12, the RPC polyline of the proposed algorithm is located at the top of the line graph, indicating that the recall rate and precision are higher. The initial value of the proposed algorithm is 60%. The recall rate in the previous stage rises linearly and is stable in the later stage, being about 97%, and the maximum precision is 99%; the initial value of the method given in paper [4] and the method given in paper [5] is about 8%, the maximum precision of the method given in paper [4] is about 75%, and the maximum precision of the method given in paper [5] is about 64%. The recall rate and precision of the three algorithms are compared, indicating that the RPC performance of the proposed algorithm is better. In the process of local edge feature extraction of super-resolution images, the proposed algorithm has a high recall rate and high accuracy. Similar to the testing set T_I , the feature extraction result obtained by the algorithm on T_{II} has a high recall rate and high precision, which has advantages.

It can be seen from Tables 1 and 2 that in the process of local edge feature extraction of super-resolution images when the proposed algorithm maintains the highest accuracy, the feature extraction time is the shortest. The reason why the algorithm has good RPC performance and F -measure performance is because the algorithm uses the Chamfer matching metric to extract the local edge features of super-resolution images. Chamfer's distance is used to measure the similarity of two-edge graphics and search for similar graphics. The Chamfer distance matching is realized by searching the minimum Chamfer distance of similar graphics. Finally, the local edge features of super-resolution images are extracted based on the local edge feature function of class Chamfer distance. The obtained features are comprehensive and accurate, which provide favourable conditions for extracting the final feature points and prevent feature points from loss.

5. Conclusions

In super-resolution image processing technology, feature extraction algorithms have attracted a great attention as a potential area of interest. The feature point extraction algorithm for the local edge of super-resolution image based on edge point has been proposed. The proposed method considers the case where the edge line is closed. The obtained

local edge feature points of the super-resolution image are lone convex points with large curvature on the edge line. The problem proposes a new fast extraction algorithm for extracting local edge features of super-resolution images. The experimental results show that the proposed algorithm can not only detect the points with large curvature on the edges of the image but also locate them accurately for refined extraction of the features. The equal error measure for extracting the local features of the super-resolution image is 96.3%, and the average time taken by the algorithm to produce the results is 0.02 seconds. In the final results, it shows a precision of 98% where our method outperforms the existing approaches, which shows accuracy of 75% and 64%, respectively, during comparative study. The proposed method is of great significance for the recognition of objects in the super-resolution image and for the reconstruction of the three-dimensional surfaces where accurate extraction of features plays a noteworthy role.

Data Availability

The data used to support the findings of this study are available from the corresponding author upon request.

Conflicts of Interest

The authors declare that no conflicts of interest exist regarding the publication of this paper.

References

- [1] G. Kumar and P. K. Bhatia, "A detailed review of feature extraction in image processing systems," in *Proceedings of the 2014 4th International Conference on Advanced Computing & Communication Technologies*, pp. 5–12, Rohtak, India, February 2014.
- [2] J. Guo, L. Liu, W. Song, C. Du, and X. Zhao, "The study of image feature extraction and classification," in *Proceedings of the 2017 International Conference on Progress in Informatics and Computing (PIC)*, pp. 174–178, Nanjing, China, December 2017.
- [3] M. C. Popescu and L. M. Sasu, "Feature extraction, feature selection and machine learning for image classification: a case study," in *Proceedings of the 2014 International Conference on Optimization of Electrical and Electronic Equipment (OPTIM)*, pp. 968–973, Bran, Romania, May 2014.
- [4] P. Hou, "A new feature extraction method for medical images integrity verification," in *Proceedings of the 2018 IEEE 4th International Conference on Computer and Communications (ICCC)*, pp. 1589–1593, Chengdu, China, December 2018.
- [5] S. Patil and S. R. Patil, "Enhancement of feature extraction in image quality," in *Proceedings of the 2019 3rd International conference on I-SMAC (IoT in Social, Mobile, Analytics and Cloud) (I-SMAC)*, pp. 490–495, Palladam, India, December 2019.
- [6] P. Benagi, S. M. Meena, U. Kulkarni, and S. Shetty, "Feature extraction and classification of heritage image from crowd source," (*ICCTCT*), in *Proceedings of the 2018 International Conference on Current Trends towards Converging Technologies*, pp. 1–5, Coimbatore, India, March 2018.

- [7] F.-P. An and X.-W. Zhou, "BEMD-SIFT feature extraction algorithm for image processing application," *Multimedia Tools and Applications*, vol. 76, no. 11, pp. 13153–13172, 2017.
- [8] S. H. Abdulhussain, A. Rahman Ramli, B. M. Mahmmud et al., "A fast feature extraction algorithm for image and video processing," in *Proceedings of the 2019 International Joint Conference on Neural Networks (IJCNN)*, pp. 1–8, Budapest, Hungary, July 2019.
- [9] E. Xi, "Image feature extraction and analysis algorithm based on multi-level neural network," in *Proceedings of the 2021 5th International Conference on Computing Methodologies and Communication (ICCMC)*, pp. 1062–1065, Erode, India, April 2021.
- [10] B. Yang, "Image feature extraction algorithm based on random deep neural network," in *Proceedings of the 2021 3rd International Conference on Intelligent Communication Technologies and Virtual Mobile Networks (ICICV)*, pp. 863–867, Tirunelveli, India, February 2021.
- [11] Y. Luo, H. Zhou, Q. Tan, X. Chen, and M. Yun, "Key frame extraction of surveillance video based on moving object detection and image similarity," *Pattern Recognition and Image Analysis*, vol. 28, no. 2, pp. 225–231, 2018.
- [12] G. Yasmin, S. Chowdhury, J. Nayak, P. Das, and A. K. Das, "Key moment extraction for designing an agglomerative clustering algorithm-based video summarization framework," *Neural Comput & Applic*, 2021.
- [13] X. Peng, X. Zhang, Y. Li, and B. Liu, "Research on image feature extraction and retrieval algorithms based on convolutional neural network," *Journal of Visual Communication and Image Representation*, vol. 69, p. 102705, 2020.
- [14] A. D. Dondekar and B. A. Sonkamble, "Analysis of flickr images using feature extraction techniques," in *Proceedings of the 2019 IEEE 4th International Conference on Computer and Communication Systems (ICCCS)*, pp. 278–282, Singapore, February 2019.
- [15] N. Werghi, S. Berretti, and A. del Bimbo, "The mesh-LBP: a framework for extracting local binary patterns from discrete manifolds," *IEEE Transactions on Image Processing*, vol. 24, no. 1, pp. 220–235, 2015.
- [16] M. Kaur and S. Kadam, "Bio-inspired workflow scheduling on HPC platforms," *Tehnički glasnik*, vol. 15, no. 1, pp. 60–68, 2021.
- [17] L. Jiang, S. R. Sakhare, and M. Kaur, "Impact of industrial 4.0 on environment along with correlation between economic growth and carbon emissions," in *International Journal of Systems Assurance Engineering and Management*, Springer Science and Business Media LLC, Berlin, Germany, 2021.
- [18] Y. Aliyari Ghassabeh, F. Rudzicz, and H. A. Moghaddam, "Fast incremental LDA feature extraction," *Pattern Recognition*, vol. 48, no. 6, pp. 1999–2012, 2015.
- [19] H. Y. Cui, J. F. Cao, H. Shi, and E. C. Bacharoudis, "Semantic-based retrieval using various visual features for real-world images," *Journal of Mechanical Engineering Research and Developments*, vol. 39, no. 2, pp. 324–339, 2016.
- [20] S. Wang, W. Guo, T.-Z. Huang, and G. Raskutti, "Image inpainting using reproducing kernel Hilbert space and Heaviside functions," *Journal of Computational and Applied Mathematics*, vol. 311, pp. 551–564, 2017.